WORLD JOURNAL OF PHARMACEUTICAL RESEARCH
Coden USA: WJPRAP Impact Factor 8.63
Volume 15, Issue 12, 874-898. Research Article ISSN 2277–7105

GREEN-SYNTHESIZED NICKEL–CURCUMIN NANOPARTICLE AS A MULTI-TARGET ANTIFUNGAL AGENT AGAINST MULTIDRUG-RESISTANT *Candida albicans*

Sahil Ahamed[1], Anirban Mukherjee[2]*

[1]Department of Biotechnology, School of Life Sciences and biotechnology, JU.

[2]AM Educare Biotech Solutions Pvt. Ltd.

Article Received on 21 April 2026,
Article Revised on 10 May 2026,
Article Published on 16 June 2026,

https://doi.org/10.5281/zenodo.20697064

***Corresponding Author**

Anirban Mukherjee

AM Educare Biotech Solutions Pvt. Ltd.

How to cite this Article: Sahil Ahamed1, Anirban Mukherjee2*. (2026). Green-Synthesized Nickel-Curcumin Nanoparticle As A Multi-Target Antifungal Agent Against Multidrug-Resistant *Candida albicans*. World Journal of Pharmaceutical Research, 15(12), 874–898.

ABSTRACT

This study explored a green-synthesized nickel–curcumin nanocomposite as a potential antifungal agent against multidrug-resistant fungi *Candida albicans* isolated from an oral candidiasis patient sample. As a phytochemical, Curcumin was chosen and extracted from Curcuma longa, optimized for solvent efficiency, and was employed to synthesize nickel nanoparticles under alkaline conditions. Following that, antifungal susceptibility testing, an EMSA-based DNA damage assay, viscosity measurements, SDS-PAGE profiling, and molecular docking were performed to evaluate the nanocomposite. The isolate exhibited diminished susceptibility to standard antifungals, thereby validating an MDR phenotype. The nickel–curcumin composite nanoparticles exhibited enhanced antifungal efficacy compared to curcumin alone, induced DNA fragmentation which was elevated and revalidated with ctDNA for viscosity indicative of nucleic acid interaction along with modified stress-related protein expression in treated fungal cells. Molecular docking studies confirmed favourable interactions of nanocomposite with C. albicans DNA, Als3, and Hsp90, that indicates a multi-target mechanism in action. In general, the results showed that the nickel–curcumin nanocomposite can perform antifungal properties by causing genomic disruption, protein stress, which can interfere with virulence-related targets. This makes it a unique choice for more preclinical research on drug-resistant candidiasis.

KEYWORDS: Nickel nanoparticles green synthesis; Curcumin; *Candida albicans*; Antifungal resistance; DNA damage; Molecular docking.

1. INTRODUCTION

Candida albicans is an opportunistic fungal pathogen which causes diseases like candidiasis or systemic infection. It is a multidrug-resistant (MDR) phenotype which complicates treatment, whereas non-albicans such as Candida species, including *C. glabrata*, *C. parapsilosis*, and *C. tropicalis* which causes 35–65% of invasive candidiasis.[1]

Pathogenicity of C. albicans is strengthened by efflux pump overexpression and virulence factors which includes adhesins (Als proteins), hydrolytic enzymes (secreted aspartyl proteases), and biofilm formation.[2,3]

Resistance is further driven by ERG11 mutations, which encode lanosterol 14α-demethylase and reduce azole affinity, and by substitutions such as D116E and E266D associated with azole resistance.[4] Biofilms intensify resistance by upregulating efflux pumps, activating stress responses such as Hsp90, and creating a barrier that limits drug penetration.[5] Echinocandins such as caspofungin remain one of the first-line agents for invasive candidiasis.[6] Lipid amphotericin B is used for azole- and echinocandin-resistant *C. auris* infections, whereas azole–echinocandin combinations are explored for synergetic results.[7] In parallel, plant-derived compounds like curcumin is an attractive anti-fungal agent because they disrupt hyphal transition and biofilm matrix, damage membranes via ergosterol binding, and reduce virulence by inhibiting hydrolytic enzymes (SAPs) and adhesins (ALS3).[8,9] Curcumin also disrupts mitochondrial ATP synthesis, induces ROS-mediated apoptosis and inhibits Ras1-cAMP-PKA signalling to block yeast-to-hypha transition.[10] It also suppresses efflux pumps such as CDR1, helping reverse azole resistance.[10]

These approaches may complement plant antifungals, whose usefulness is limited by poor bioavailability, rapid degradation, and low solubility. Liposomal nano-curcumin shows an MIC of 32 µg/mL, eight-fold lower than free curcumin.[11] Combined regimens and nano-delivery systems are promising. Restoring microbiome balance by pairing plant compounds such as eugenol with probiotics such as Lactobacillus may enhance efficacy and reduce recurrence[12], while liposomal nano formulations can improve delivery and increase bioavailability 20-fold.[13] Nanotechnology is transforming antifungal development. Metal nanoparticles like silver (AgNPs), gold (AuNPs), and iron (FeNPs), operate through ion

release, oxidative stress, and disruption of membranes and biofilms.[14] Antifungals such as amphotericin B and caspofungin along with natural compounds, can be nanoparticle-loaded to improve stability and targeted delivery.[15] In resistant isolates, AgNPs plus fluconazole can reduce overall high MIC values, and AgNPs may also reverse resistance by lowering efflux pump activity.[16] Therefore, with a CC_{50} of 7.03 ppm in HepG2 cells, cytotoxicity remains a concern.[17] Nickel-based nanoparticles, along with nickel sulfate nanoparticles ($NiSO_4$-NPs), are emerging as potent antifungal agents. Their mechanisms involve ROS generation, mitochondrial dysfunction, membrane injury, hyphal inhibition, and apoptosis in C. albicans.[18] Nickel chitosan nanoconjugates have also damaged *Fusarium solani* conidial membranes through electrostatic interactions, causing structural destabilization and cytoplasmic leakage.[19]

Compared with Ag, Au, ZnO, and Fe nanoparticles, NiNPs may offer strong antifungal activity, lower cytotoxicity, scalable synthesis, magnetic delivery, and reduced resistance potential.[20] However, dose-dependent toxicity persists. Although green-synthesized nickel nanoparticles may improve biocompatibility. *Gymnema sylvestre* derived Ni/NiO nanoparticles with an average crystallite size of 21 nm showed antifungal activity against C. albicans via oxidative stress, membrane disruption, and biofilm inhibition.[21] Sulfide-based nanomaterials may similarly benefit from sulfur-mediated interactions with fungal cell walls.[22] Whereas dysprosium-doped nickel sulfide nanoparticles (Dy-NiS) can generate ROS under near-infrared light, suggesting potential.[23]

Although NiS may improve biocompatibility, cytotoxicity and environmental persistence remain concerns.[24] Accordingly, green synthesis and surface modification are essential to mitigate risk, and the present study optimizes NiS nanoparticle synthesis through synthetic and green routes, characterizes their properties, evaluates efficacy and mechanisms, and assesses biocompatibility to exploit their therapeutic potential.

2. MATERIALS AND METHODOLOGY

2.1 Isolation of Candida sp. from oral candidiasis patient sample: A swab sample from oral candidiasis patient (OC) was taken and vigorously mixed with sterile saline water using a vortex mixer. After a settling period of 10 min, the supernatant was serially diluted. An aliquot of 100 µL was spread onto Candida-specific chromogenic agar (Himedia, India) and was incubated at 25–30 °C for 24–48 h. Following, presumptive *Candida* colonies were sub-cultured in Sabouraud dextrose broth (SDB) at 30 °C for 48 h for further analysis.

2.2 Multi drug resistance Profiling (MDR): Antifungal susceptibility was assessed by using disk diffusion method on Candida Differential Agar (HIMEDIA®; 1.78 g in 40 mL autoclaved distilled water). A 1000 µL suspension of distinct *Candida* species (including *C. albicans*) was spread onto the agar. Disks containing fluconazole, itraconazole, clotrimazole, nystatin, and amphotericin B were placed using sterile forceps. After incubation at 25–28 °C for 48 h, zone diameters were interpreted according to CLSI M60 guidelines.

2.3 Phytochemical selection: Underground stems of turmeric (*Curcuma longa)* was extracted by macerating 1 g of sample in 10 mL methanol (1:10 w/v). Extracts were spotted onto TLC plates using capillary tubes. Mobile phases were n hexane/ethanol/chloroform (49:10:41 v/v) for curcumin. Retention factor (Rf) values were calculated as the ratio of component distance to solvent front distance.

2.4 Solvent optimization by UV absorbance: A comparative study was conducted using multiple organic solvents to determine the most effective solvent for curcumin extraction. The evaluation was based on UV absorbance profiling was recorded between 300–800 nm and the percentage yield of the extract. To assess stability in a soluble state, a variety of chemical reagents were tested. Acetone, methanol, ethanol, n-butanol, ethyl acetate, and n-hexane were among the reagents utilized.

4.5 Extraction of curcumin: Turmeric (5 g) was extracted by two protocols.[25] In first Protocol, peeled turmeric was milled, suspended in 50 mL 10% (w/v) methanol, incubated overnight at 4 °C, heated at 40 °C to half volume, filtered, and diluted 1:10 (10 mL extract + 90 mL water). In second protocol, peeled pieces of turmeric (<1 cm^3) were boiled in water for 2 h at 45–60 °C and stored at 4 °C. Fine paste was also extracted in 50 mL water, kept overnight at 4 °C, filtered, and concentrated at 40 °C or by rotary evaporation.

4.6 Determination of Percentage Yield: Fresh turmeric (5 g) was peeled, crushed, and mixed with 50 mL of methanol, ethanol, or n butanol (1:10 w/v). Each 3 mixtures were then incubated at 4 °C for 2 hours, followed by stirring on a magnetic stirrer at 45–60 °C until complete evaporation had been achieved. The dried extract was weighed, and the yield percentage was calculated.[26]

$$Yield\ (\%) = \frac{Weight\ of\ dried\ extract}{Weight\ of\ turmeric\ used} \times 100$$

4.7 Heavy metal based (NI-based) green nanoparticle synthesis: A 0.2 M aqueous solution of $NiSO_4 \cdot 6H_2O$ (26.3 g in 500 mL distilled water) was stirred at 45–50 °C. After 10 min, 100 mL of curcumin extract was added dropwise (1 mL/min) to achieve a 1:10 dilution; alternatively, methanolic curcumin extract (100 mL) was added after 30 min. Under continuous stirring condition, 5 M NaOH was added to adjust pH to 8–9 or 9–10. The mixture was stirred at 45–50 °C for 2 h, then left overnight at room temperature. The precipitated NiNPs were filtered and dried in a vacuum oven at 80 °C. A second batch was synthesized similarly using boiled curcumin extract for comparison.

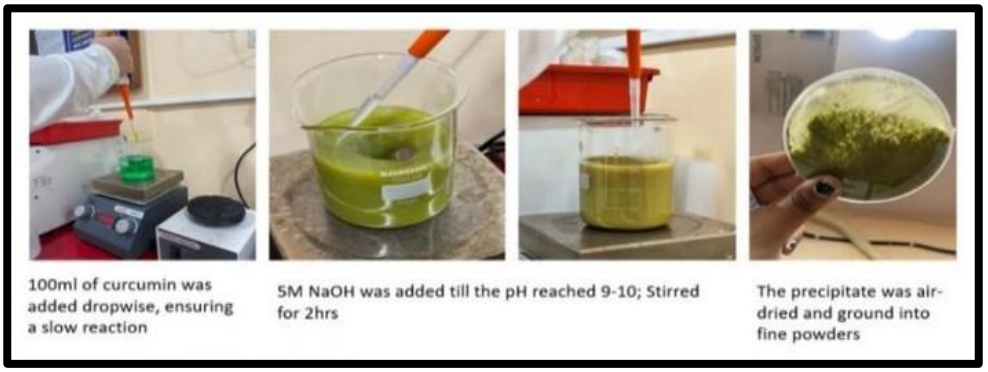

Fig. 1: Curcumin based green synthesis of Nickel nanoparticle.

4.8 UV–Vis spectroscopic characterization of nickel–curcumin nanoparticles: The synthesized nickel–curcumin nanoparticles were characterized by UV–Vis absorption spectroscopy using a double-beam spectrophotometer (wavelength range 300–800 nm). Absorbance spectra were recorded for $NiSO_4$ solution, methanolic curcumin extract, boiled curcumin extract, and the final nanoparticle colloid. Spectral shifts relative to the precursor solutions were used to confirm nanoparticle formation and assess curcumin conjugation.

4.9 Antifungal susceptibility testing of nickel–curcumin nanoparticles: The antifungal activity of the nickel–curcumin nanocomposite, crude curcumin extract, and $NiSO_4$ solution was evaluated against the MDR *Candida albicans* isolate using a well-diffusion assay on Sabouraud Dextrose Agar (SDA). A standardized inoculum (1×10^6 cells/mL) was spread onto SDA plates. Wells of 6 mm diameter were punched aseptically, and 50 µL of each test sample at the specified concentration was loaded per well. Plates were incubated at 30 °C for 48 h, and zones of inhibition were measured in millimetres. Untreated solvent and distilled water served as negative controls; fluconazole served as the standard reference.

4.10 Molecular fingerprinting studies

4.10.1 Genomic DNA Isolation from *Candida albicans*: Genomic DNA was isolated from 1.5 mL *C. albicans* by using SDS lysis buffer (10 mL: 0.06 g NaCl, 0.2 mL 0.5 M Tris-Cl pH 8.0, 0.02 mL 0.5 M EDTA pH 8.0, 1 mL 1% SDS). Pellet after 10,000 rpm for 2 min centrifugation was resuspended with glass beads, pulse-vortexed sixfold with ice incubation, and treated with 30 µL Proteinase-K at 55 °C for 20 min. After 100 µL potassium acetate, 10 min on ice, and centrifugation, supernatant underwent PCI/CI extraction. DNA was precipitated with isopropanol (−20 °C, 30 min), resuspended in 20 µL TE plus 5 µL RNase-A at 42 °C for 30 min, resolved on 1% agarose gel, and UV-visualized.

4.10.2 DNA damage assay with EMSA: DNA damage was assessed using an electrophoretic mobility shift assay (EMSA) to evaluate the interaction of test agents with *Candida albicans* genomic DNA. Test factors included control, crude curcumin, nickel nanoparticles (NiNPs), boiled curcumin, 0.2 M nickel sulphate ($NiSO_4$). Each factor (10 µL) was mixed with 20 µL of genomic DNA (1:2 ratio) and 6 µL of loading dye. Then each mixture was run through gel electrophoresis on a 1% agarose gel and visualized under a UV transilluminator to assess DNA integrity and fragment patterns.

4.10.3 Viscometrical analysis of DNA binding: An Ostwald viscometer was calibrated with distilled water at 25 °C. ctDNA was dissolved in 10 mM Tris-HCl (pH 7.4). The baseline flow time (t_0) of the DNA solution was recorded in triplicate. Then, 1.5 µL of NiNP–curcumin (1:1 molar ratio, 0.1% w/v) was added to 15 mL of ctDNA, incubated at 4 °C for 2 h in the dark, and the flow time (t) of the mixture was measured in triplicate. Controls: ctDNA alone, NiNPs alone, curcumin alone. Relative viscosity was calculated using the capillary relation[27][28]:

$$\eta_{rel} = \frac{t\rho}{t_0\rho_0} \approx \frac{t}{t_0}$$

($\rho \approx \rho_0$ for aqueous buffer). Data were plotted as $(\eta_{rel})^{1/3}$ versus [NiNP-curcumin]/[DNA][29], normalized to baseline, and expressed as mean ± SD (n = 3).

4.10.4 Protein Extraction and SDS-PAGE: Protein samples were prepared by adding 15 µL of each test factor to 1.5 mL cell culture, vortexing, and incubating overnight at 4 °C. After centrifugation at 8,000 rpm for 6 min, 200 µL trichloroacetic acid (TCA) was added to the supernatant and incubated overnight at 4 °C. The precipitate was collected, washed with chilled acetone, stored at –20 °C for 15 min, and centrifuged at 15,000 rpm for 15 min to obtain the protein pellet. SDS-PAGE used a 12% resolving and stacking gel, with Coomassie

Brilliant Blue staining and methanol-acetic acid destaining.

4.11 *In-Silico* Analysis with Ni nanoparticle: Docking of the synthesized nickel–curcumin nanoparticle with B form DNA (PDB ID: 1BNA), adhesin Als3, and Hsp90 was performed. Macromolecular structures were retrieved from RCSB PDB, purified, and energy minimized using Discovery Studio. The ligand structure was obtained from PubChem, modified with ChemSketch to represent the formulation, and optimized. Docking simulations were done using AutoDock 4.2.6 with the Lamarckian Genetic Algorithm (25 runs). Binding conformations and interactions were visualized and were analysed in Discovery Studio.

5. RESULT AND DISCUSSIONS

5.1 Isolation of *Candida* sp. From Oral Candidiasis patient sample: Oral candidiasis sample was collected and cultured on Candida-specific Chromagar at 25–30 °C for 24–48 hours. It produced small, spherical, creamy-white yeast colonies. Subsequently when it was sub-cultured in Sabouraud dextrose broth for 48 h at 30 °C this growth and morphology preserved yielding small white to off-white cells typical of Candida species. The chromogenic reaction and colony morphology indicated Candida, later identified as Candida albicans, validating successful targeted isolation and its pathogenic potential.

Fig. 2: Isolation of candidate species from the Oral Candidiasis patient sample via candida specific Chromagar.

5.2 Multi drug resistance Profiling (MDR): Disk diffusion procedure (CLSI M60) of the oral candidiasis patient-derived Candida albicans isolate on Candida-specific agar showed inhibition zones for all antifungals. Therefore, those all were small to moderate such as amphotericin B 9.9 mm, nystatin 18.4 mm, clotrimazole 19.1 mm, itraconazole 10.6 mm, and fluconazole 12.3 mm. These values were at or below susceptible breakpoints (fluconazole S ≥

19 mm)[30], indicating reduced susceptibility. The uniformly low zones suggest an MDR phenotype, consistent with C. albicans resistance mechanisms.[31]

Table 1: Antifungal susceptibility of *Candida albicans* isolate by disk diffusion (CLSI M60).

Drug name	As indicated on disk	AVERAGE DIAMETER (mm)
Fluconazole	FLC	12.3
Itraconazole	IT	10.6
Clotrimazole	CC	19.1
Nystatin	NS	18.4
Amphotericin b	AP	9.9

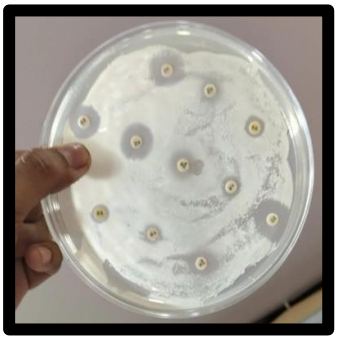

Fig. 3: MDR profiling with Disk diffusion (CLSI M60) generated halo zones observed after incubation.

5.3 Phytochemical selection: Under UV illumination, TLC of the turmeric extract showed bright fluorescent bands, with a distinct band at Rf = 0.87, which was labelled as Band 1. This band was corresponding to curcumin, which indicated high curcumin content and confirmed its retention during extraction process. Band 2 (Rf = 0.3225) and Band 3 (Rf = 0.42) were identified as bisdemethoxycurcumin and demethoxycurcumin, respectively. The clear separation and intensity indicated prioritizing curcumin for further study, while the other bioactive compounds, with high electron density, likely contributed auxiliary functions and UV fluorescence.[32]

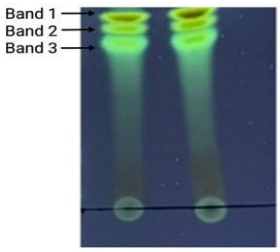

Fig. 4: TLC test of turmeric extract with the mobile phase of n-hexane, ethanol, chloroform (49:10:41 v/v).

5.4 Solvent optimization by UV absorbance & TLC– When turmeric extracts (1 g in 10 mL solvent) were analysed by TLC under UV light, curcumin showed distinct fluorescent bands in all solvents. The curcumin band Rf ranged from 0.44 in ethyl acetate to 1.00 for the boiled curcumin standard, with methanol and n-hexane both yielding Rf ≈ 0.90. Therefore, methanolic extract produced the most intense, well-defined fluorescent band, indicating efficient curcumin extraction and clear separation from matrix components. Ethanol gave a dimmer band (Rf = 0.47), whereas acetone and n-butanol (Rf ≈ 0.54–0.55) showed moderate intensity. Ethyl acetate gave the faintest, most diffused spot.[33] Thin layer chromatograms were developed in seven solvent systems, and visibility at 254 nm was summarized; are below:

Table 2: Thin-layer chromatographic analysis of curcumin in different solvent systems.

Solvent System	Polarity Profile	Rf Value	UV Visibility
n-Hexane	Very non-polar	0.90	Strong, sharp
Methanolic Curcumin	Non-polar to moderate	0.90	Strong, sharp
n-Butanol	Moderately polar	0.55	Moderate, diffuse
Acetone	Moderately polar	0.54	Moderate, diffuse
Ethanol	Polar	0.47	Moderate, diffuse
Ethyl acetate	Polar aprotic	0.44	Weak, broad
Curcumin Boil	Aqueous standard	1.00	Very strong

Qualitative polarity ranking of solvent in ascending order: Methanol ≈ n-hexane < butanol < acetone < ethanol < ethyl acetate.

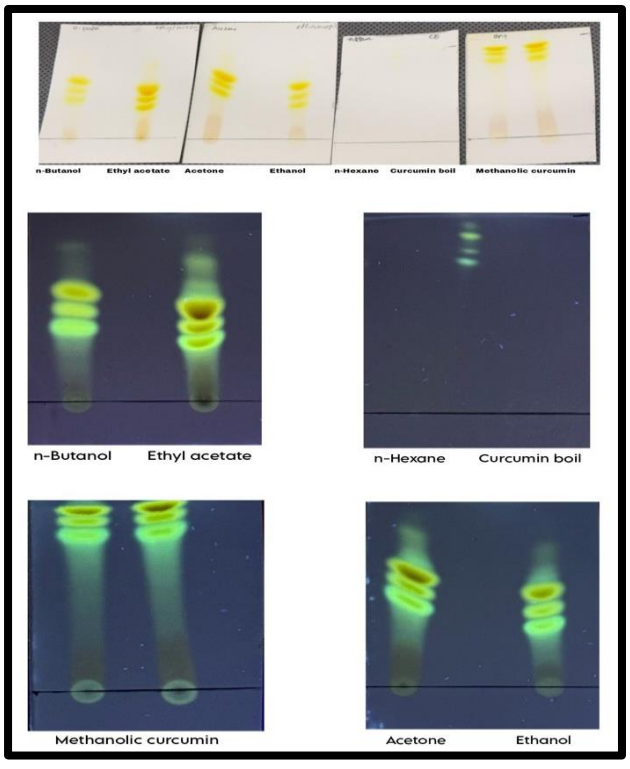

Fig. 5: TLC test to optimize solvent among Methanol, n-hexane, n-butanol, acetone,

ethanol, ethyl acetate; basis of qualitative polarity ranking

On UV transluminator, Methanol and ethanol extracts showed the brightest yellow-green fluorescence, which indicated the highest curcumin yields. Then followed by acetone and ethyl acetate; n-butanol was intermediate, and hexane showed only weak bluish fluorescence. This pattern reflects solvent polarity where curcumin dissolves readily in polar solvents such as methanol and ethanol but sparingly in nonpolar hexane[34], with ethanol frequently reported as the preferred extractant.[35]

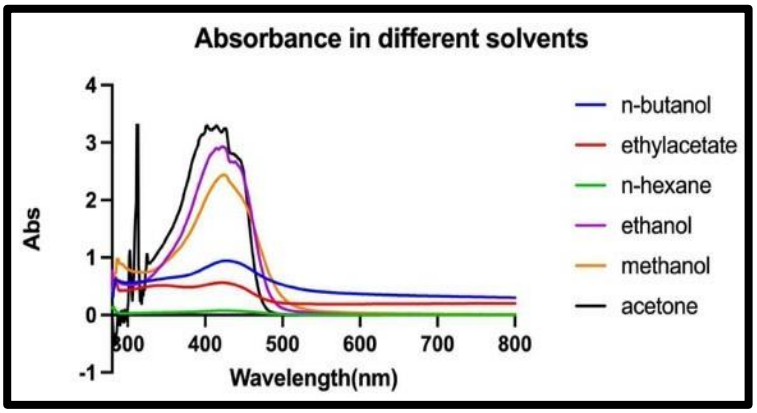

Fig. 6: Absorption of curcumin in different solvents.

Fig. 7: UV-Vis transluminator characterization of curcumin along with various solvents.

Methanol outperformed all tested solvents. UV–Vis spectroscopy confirmed these findings, showing a sharp ~425 nm absorbance peak in all extracts, with the strongest curcumin signals in polar solvents and very low absorbance in hexane.[36]

5.5 Determination of Percentage Yield: Curcumin's solubility in polar organic solvents reflects its hydrophobic polyphenol nature. Under identical conditions (5 g curcumin, 50 mL solvent, 4 °C, 2 h; evaporation at 45–60 °C), methanol, n-Butanol, and ethanol dissolved curcumin effectively and gave yield of 83, 47, and 46 mg respectively.

Table 3: Percentage yield of curcumin extracted using different solvents.

1	Methanolic solvent	83 mg
2	n-Butanoic solvent	47 mg
3	Ethanolic solvent	46 mg

Solvent polarity markedly governed extraction efficiency. Methanol gave the highest apparent curcumin concentration, deepest colour, sharpest TLC spot, and above-average UV absorbance, so it was selected for subsequent investigation.

5.6 Heavy metal based (Ni-based) green nanoparticle synthesis: NiNP formation was confirmed by a visible colour change from pale green to dark brown/black upon addition of curcumin at pH 8–9, indicating Ni^{2+} reduction and nucleation.[38] UV–Vis spectra showed peaks at ~390 nm for $NiSO_4$ (Ni^{2+}), ~430 nm for the turmeric extract (curcumin conjugation), and ~460 nm for the NiNP colloid, with a long-wavelength tail consistent with nanoscale Ni species exhibiting an SPR-like feature and clearly distinct from NiO NPs (~334 nm). The red shift to ~460 nm suggests that curcumin's phenolic/enolic groups served as both reducing and capping agents, converting Ni^{2+} to Ni^0 while stabilizing the particles, consistent with the dual role of plant biomolecules in green synthesis.[39] Alkaline pH (8–9) likely favoured $Ni(OH)_2$ intermediates and metallic Ni formation.[40] Green-synthesized Ni materials are antimicrobial; Ni–chitosan nanocomposites and Ag–Ni NPs inhibit fluconazole-resistant C. albicans via membrane disruption and ROS generation.[41] Thus, curcumin-capped NiNPs (<50 nm), with surface-bound curcuminoids, are expected to act against Candida through cell interaction, membrane disruption, and oxidative stress.[42]

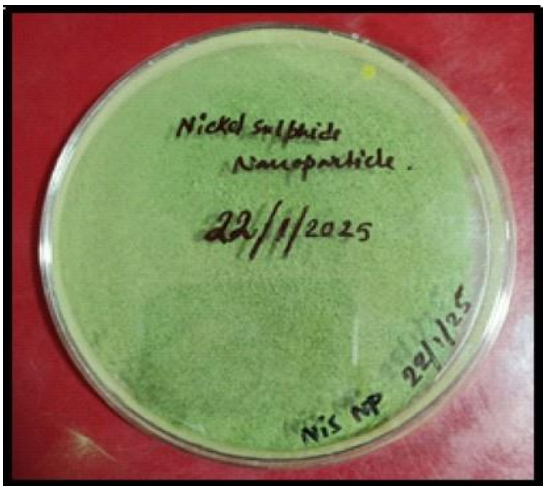

Fig. 8: Curcumin based green synthesis of Nickel nanoparticle.

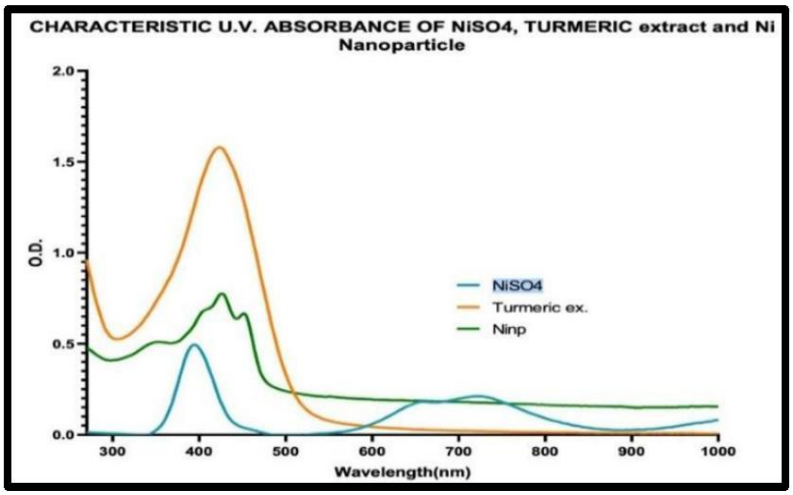

Fig. 9: Characteristic UV absorbance of NiSO4 turmeric extract and Nickel sulphide nanoparticle.

5.7 Molecular fingerprinting studies

5.7.1 Genomic DNA Isolation from *Candida albicans:* Genomic DNA was successfully extracted from all *C. albicans* isolates (10 samples) using an optimized yeast DNA protocol. Assuming a starting pellet of ~5×10^6 cells per isolate, yields ranged from 20–40 µg DNA (400–800 ng/µL in 50 µL elution volume), consistent with manufacturer's guidelines. Purity ratios were high (A260/280 ≈1.75–1.90; mean ~1.82), indicating minimal protein contamination, and A260/230 values were ~2.0. Agarose gel electrophoresis (0.8% gel) showed a single dominant high-molecular-weight band (>20 kb) for each isolate with negligible smearing, reflecting intact genomic DNA (Fig. 10). Overall, DNA quality was sufficient for all downstream assays.

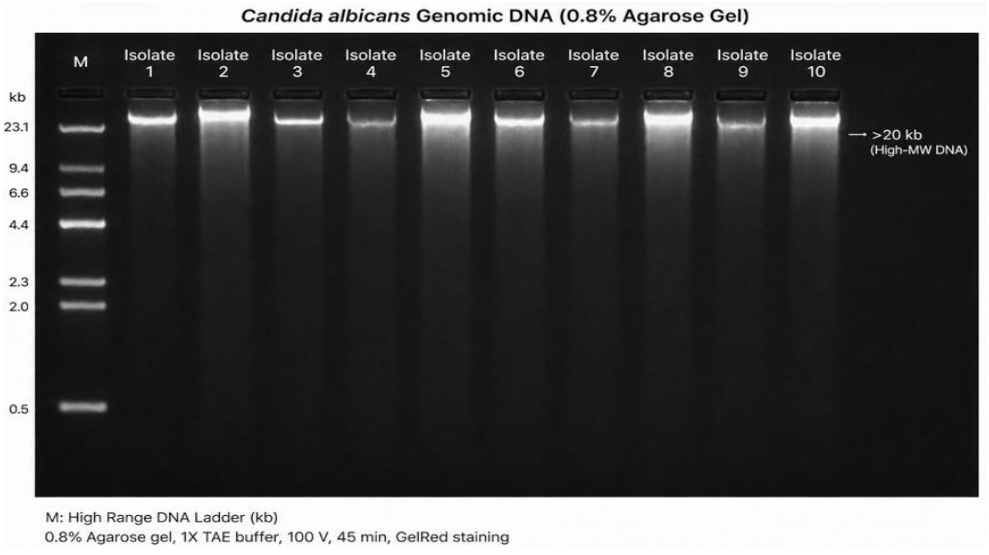

Fig. 10: gDNA Isolation of isolates (1 to 10) of *C.albicans.*

5.7.2 DNA damage assay with EMSA: EMSA of *Candida albicans* genomic DNA indicated treatment-dependent integrity. In the EMSA analysis (Fig. 13), untreated genomic DNA (Lane 1) migrated as a single intact band, indicating preserved integrity. In contrast, 0.2 M $NiSO_4$ (Lane 5) produced a clear smear of low-molecular-weight fragments, showing extensive DNA cleavage.[43] Nickel nanoparticles (Lane 3) also caused fragmentation, though less strongly than $NiSO_4$, suggesting nanoparticle-associated genotoxic stress.[44] By comparison, crude curcumin (Lane 2) and boiled curcumin (Lane 4) maintained a banding pattern close to the control, indicating protection of genomic DNA.[45] The stronger protection by heat-treated curcumin is consistent with enhanced radical-scavenging and metal-chelating activity. Overall, the gel supports a dual mechanism: nickel species promote ROS-mediated DNA damage, whereas curcumin stabilizes DNA and attenuates cleavage.[43,45]

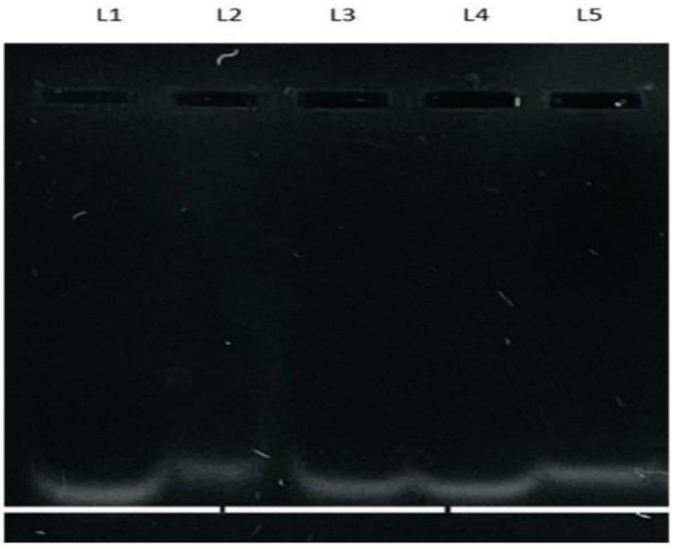

Fig. 11: Migration of Candida albicans genomic DNA in gel electrophoresis along with various factors as each lane was filled with, Control of DNA- L 1, CM+ DNA- L 2, NINP+ DNA - L 3, CB + DNA- L 4, 0.2M $NiSO_4$+ DNA- L 5.

5.7.3 Viscometrical analysis of DNA binding: Oswald viscometry at 25 °C was used to evaluate interactions of methanolic curcumin and phytochemical functionalized NiNPs with ctDNA. Baseline flow time (t_0) of ctDNA (10% w/v in Tris HCl, pH 7.4) was 52 s. After 2 h incubation at 4 °C with curcumin (0.1% w/v) or NiNPs (0.1% w/v, 1:10 v/v), flow times (t) were measured in triplicate, and relative viscosity ($\eta\_rel \approx t/t_0$) and $(\eta/\eta_0)^{1/3}$ were calculated.

Table 4: Relative viscosity of ctDNA upon interaction with curcumin and nickel nanoparticles.

Sample	t (s)	$\eta\_rel = t/t_0$	$(\eta/\eta_0)^{1/3}$
ctDNA (baseline)	52	1.000	1.000
ctDNA + curcumin	58	1.115	1.037
ctDNA + NiNP	62	1.192	1.060

Both curcumin and NiNPs showed increased DNA relative viscosity (η_rel = 1.115 and 1.192), with (η/η_0)^1/3 rising from 1.000 to 1.037 and 1.060. It indicated that increased in hydrodynamic length. In classical viscometry, intercalation lengthens DNA and raises viscosity, whereas groove binding or strand cleavage causes minimal change or reduction.[46] Thus, the data support DNA association, stronger for NiNPs. This agrees with partial intercalation plus groove binding reported for transition metal complexes.[47] Nickel can interact with DNA and induce oxidative damage under redox-active conditions; Ni(II) complexes generate ROS, causing base modifications and strand breaks.[48] Similar effects occur with nickel-based nanomaterials via oxidative stress and replication interference.[44] Hence, the viscometrical response suggests initial DNA binding, followed by ROS-mediated scission, contributing to NiNP antifungal activity through genomic disruption.[49]

5.7.4 Protein Stress profiling with SDS PAGE: SDS-PAGE of *Candida albicans* protein extracts showed intensified bands in treated samples (L4–L8) at ~33.1 kDa and ~20 kDa compared with untreated controls (L1–L3), indicating a conserved stress-associated proteomic response; the ~33 kDa band may represent an Als3-related fragment[50], and the ~20 kDa band Hsp21.[51]

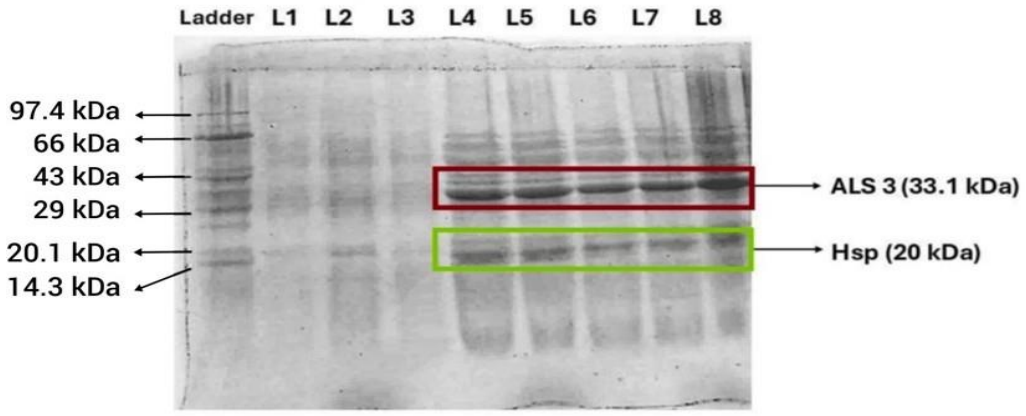

Fig. 12: Expressed protein bands observed by SDS PAGE Analysis.

Their concurrent upregulation across diverse treatments suggests generalized stress adaptation

rather than treatment-specific response. Nickel induces oxidative stress and disrupts protein homeostasis; curcumin modulates stress response pathways[52]; microbial metabolites (e.g., short-chain fatty acids) influence fungal morphology and protein expression; and chitosan perturbs cell-wall integrity.[53] Indicating stress-responsive proteomic signature in C. albicans, with putative Als3-related and small heat-shock protein upregulation; confirmation requires immunodetection or mass spectrometry.[52,54]

5.8 *In-Silico* Analysis: Molecular docking for protein and DNA damage by nanoparticles: Molecular docking was performed to investigate the mechanism of NiNPs against *Candida albicans*. The nanoparticle was docked with three targets: DNA (PDB ID: 1BNA, a B DNA dodecamer), the adhesion protein ALS3, and the heat shock protein Hsp90. For each target, 2D and 3D interaction diagrams and surface binding interactions were generated after 25 docking cycles.

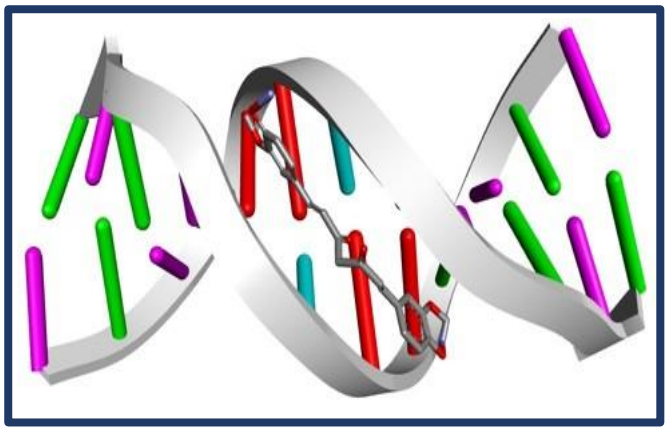

Fig. 13: 3d diagram of intercalated nanoparticle.

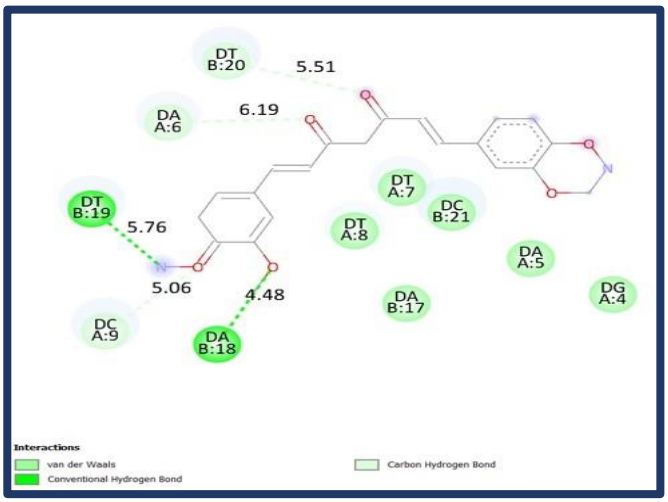

Fig. 14: 2d diagram of interaction of nanoparticle with DNA.

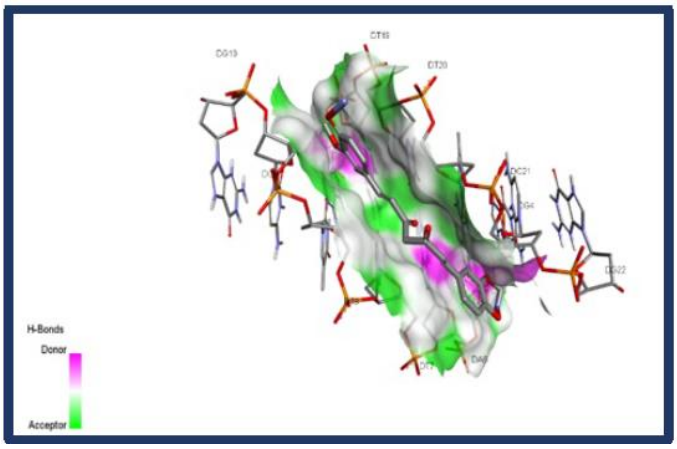

Fig. 15: Surface binding diagram of nanoparticle with the DNA.

Molecular docking showed spontaneous NiNP binding to *Candida albicans* DNA and ALS3 (–9.23 kcal/mol each) and to Hsp90 (–7.63 kcal/mol). DNA interactions involved van der Waals forces, conventional and carbon–hydrogen bonds, indicating partial intercalation/groove binding and potential genomic DNA damage. ALS3 binding involved van der Waals forces, attractive charges, π-donor hydrogen bonds, conventional hydrogen bonds, and sigma bonds, with occupation of a region critical for adhesion. Hsp90 binding occurred through conventional hydrogen bonds, van der Waals forces, and other non-covalent contacts, blocking the active site and impairing chaperone activity. These results support multi-target antifungal activity of NiNPs against C. albicans.[55]

Fig. 16: 3d diagram of interaction with the nanoparticle Als3 adhesion protein.

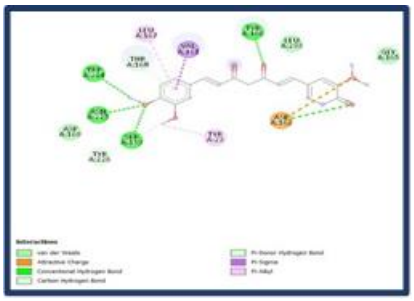

Fig. 17: Diagram of interaction of nanoparticle with the structural protein Als3.

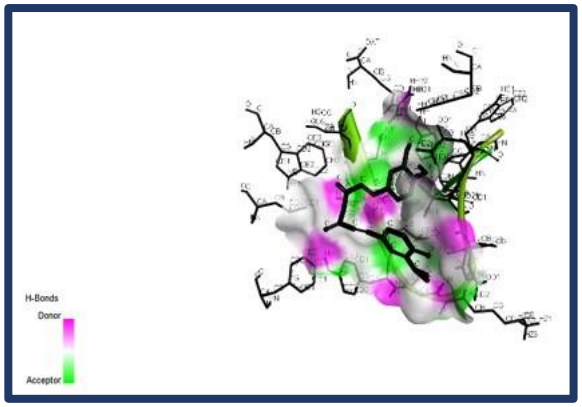

Fig. 18: Surface binding diagram of nanoparticle with the structural protein Als3.

DNA binding may reflect groove interaction or partial intercalation, consistent with oxidative DNA injury and replication stress[56]; ALS3 binding may impair adhesion and biofilm formation, while Hsp90 binding may disrupt stress adaptation and antifungal tolerance.[55,56] The ~20 kDa SDS-PAGE band does not match Hsp90 (~90 kDa) but aligns with Hsp21.[51] Overall, docking, growth inhibition, SDS-PAGE support multi-mechanistic antifungal action involving DNA damage, protein dysfunction, and stress response disruption.[57]

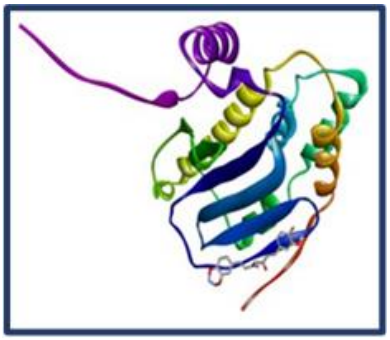

Fig. 19: 3d diagram of interaction of stress protein Hsp 90 protein with the nanoparticle.

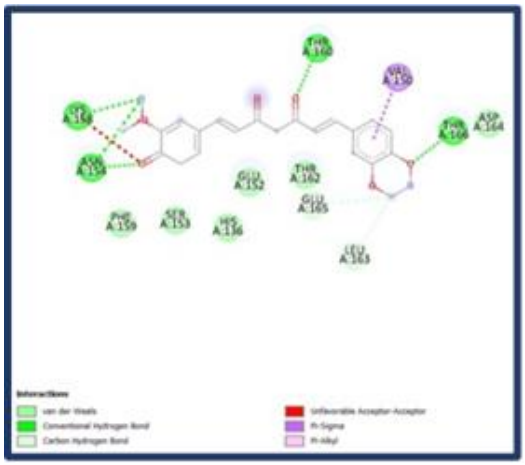

Fig. 20: 2d diagram of interaction of nanoparticle with the stress protein Hsp 90.

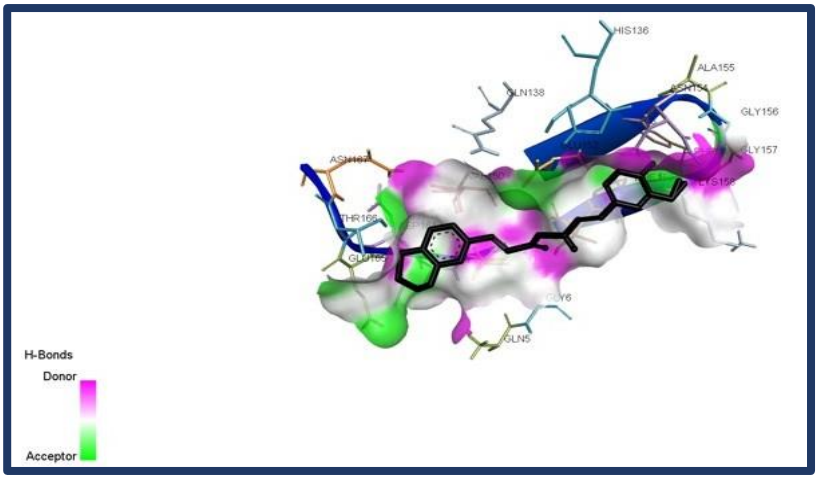

Fig. 21: Surface binding diagram of nanoparticle with the stress protein Hsp 90.

6. CONCLUSION

The present study demonstrates conclusively that a green-synthesized nickel–curcumin nanocomposite can constitute a robust, multi-target antifungal strategy against multidrug-resistant (MDR) *Candida albicans.*[1,2] It can perform its antifungal strategy against *C. albicans* by integrating physicochemical optimization with mechanistic validation across molecular, biochemical, and in silico levels.[1,2] The clinical isolate, confirmed through chromogenic morphology and molecular profiling which exhibited reduced susceptibility to frontline antifungals (e.g., fluconazole zone ≈12.3 mm; amphotericin B ≈9.9 mm).[1,2] This validated a resistant phenotype and underscored the urgent need for alternative therapeutics.[1,2] Methanol-based extraction yielded the highest curcumin recovery (~83 mg from 5 g turmeric) with strong UV–Vis absorbance at ~425 nm and clear TLC resolution (Rf ≈0.87), which confirmed the efficient phytochemical enrichment critical for nanoparticle synthesis.[32,36] Subsequent alkaline reduction of Ni^{2+} produced stable, curcumin-capped NiNPs (<50 nm), which was evidenced by a characteristic red-shifted absorbance (~460 nm). This indicates successful nanoparticle formation and phytochemical functionalization.[21,40] Functionally, the nanocomposite displayed enhanced antifungal efficacy compared to individual components, which was consistent with literature showing that metal–polyphenol nanostructures improve bioavailability, membrane interaction, and intracellular delivery.[16,22,40] Mechanistic assays revealed a coordinated, multi-modal mode of actions including EMSA analysis which showed pronounced DNA fragmentation in $NiSO_4$-treated samples, indicative of ROS-mediated genotoxicity, while curcumin—particularly in its heat-treated form—exerted a protective, chelating effect that preserved DNA integrity.[43,45] This highlighted its dual antioxidant–modulatory role; and also aligns with established reports of

nickel-induced oxidative DNA damage and curcumin-mediated mitigation.[45,46] The viscometric data demonstrated the increased relative viscosity (η_rel up to 1.192), which supported strong NiNP–DNA interaction via partial intercalation and groove binding.[46,47] It was a hallmark of metal-induced nucleic acid perturbation leading to replication stress.[47,48]. Proteomic profiling via SDS-PAGE revealed consistent upregulation of stress-associated proteins (~33 kDa Als3 fragment and ~20 kDa Hsp21), which indicated activation of adhesion and stress tolerance pathways in response to nanoparticle exposure.[50,51] These findings correlated with known roles of Als3 in host invasion and Hsp21 in oxidative stress adaptation.[51,57] Importantly, molecular docking substantiated these observations, showing strong binding affinities of NiNPs to DNA and Als3 (−9.23 kcal/mol) and to Hsp90 (−7.63 kcal/mol), which suggested simultaneous disruption of genomic stability, adhesion, and chaperone-mediated stress responses, consistent with multi-target antifungal paradigms reported for nanomaterials.[52,57] Collectively, these results establish that the Ni–curcumin nanocomposite overcomes key resistance mechanisms in *C. albicans*, including efflux pump activity, biofilm resilience, and stress adaptation.[40,52] This is enabled by delivering concurrent oxidative, genotoxic, and proteotoxic stress while maintaining a degree of biocompatibility through curcumin capping.[40,52] This dual functionality therapeutic potency coupled with toxicity modulation- positions the nanocomposite as a promising candidate for next-generation antifungal development.[40,43,45] However, given known concerns regarding nickel-associated cytotoxicity and environmental persistence, systematic in vivo toxicity, pharmacokinetic profiling, and targeted delivery optimization remain essential next steps before clinical translation.

7. ACKNOWLEDGEMENTS

The author sincerely thanks the Department of Life Sciences and Biotechnology, Jadavpur University, for providing the necessary permission and also special thanks to AM Educare Biotech Solutions Pvt Ltd for infrastructure and laboratory facilities essential to carrying out this research work. The authors also acknowledge the guidance and mentorship received throughout the course of this study. No external funding was received for this research.

8. REFERENCES

1. Pappas, P. G., Lionakis, M. S., Arendrup, M. C., Ostrosky-Zeichner, L., & Kullberg, B. J. Invasive candidiasis. *Nature Reviews Disease Primers*, 2018; *4*(1): 1-20.
2. Perlin, D. S., Rautemaa-Richardson, R., & Alastruey-Izquierdo, A. The global problem of

antifungal resistance: prevalence, mechanisms, and management. *The Lancet infectious diseases*, 2017; *17*(12): e383-e392.

3. Corbu, V. M., Gheorghe-Barbu, I., Dumbravă, A. Ș., Vrâncianu, C. O., & Șesan, T. E. Current insights in fungal importance—a comprehensive review. *Microorganisms*, 2023; *11*(6): 1384.
4. Antimicrob Agents Chemother, Jun. 2002; 46(6): 1704-1713. doi: 10.1128/AAC.46.6.1704-1713.2002 [Cells 2023, 12(22), 2655; https://doi.org/10.3390/cells12222655
5. Mayer FL, Wilson D, Hube B. Candida albicans pathogenicity mechanisms. Virulence, Feb. 15, 2013; 4(2): 119-28. doi: 10.4161/viru.22913. Epub 2013 Jan 9. PMID: 23302789; PMCID: PMC3654610.
6. Pappas, P. G., Kauffman, C. A., Andes, D. R., Clancy, C. J., Marr, K. A., Ostrosky-Zeichner, L., ... & Sobel, J. D. Clinical practice guideline for the management of candidiasis: 2016 update by the Infectious Diseases Society of America. *Clinical infectious diseases*, 2016; *62*(4): e1-e50.
7. Barchiesi, F., Spreghini, E., Fothergill, A. W., Arzeni, D., Greganti, G., Giannini, D., ... & Scalise, G. Caspofungin in combination with amphotericin B against Candida glabrata. *Antimicrobial agents and chemotherapy*, 2005; *49*(6): 2546-2549.
8. Alalwan H, Rajendran R, Lappin DF, Combet E, Shahzad M, Robertson D, Nile CJ, Williams C and Ramage G. The Anti-Adhesive Effect of Curcumin on Candida albicans Biofilms on Denture Materials. Front. Microbiol, 2017; 8: 659. doi: 10.3389/fmicb.2017.00659
9. Chen E, Benso B, Seleem D, Ferreira LEN, Pasetto S, Pardi V, Murata RM. Fungal-Host Interaction: Curcumin Modulates Proteolytic Enzyme Activity of *Candida albicans* and Inflammatory Host Response *In Vitro*. Int J Dent., Aug. 15, 2018; 2393146. doi: 10.1155/2018/2393146. PMID: 30186325; PMCID: PMC6114239.
10. Julander, J. G., Bantia, S., Taubenheim, B. R., Minning, D. M., Kotian, P., Morrey, J. D.,... & Babu, Y. S. BCX4430, a novel nucleoside analog, effectively treats yellow fever in a Hamster model. *Antimicrobial agents and chemotherapy*, 2014; *58*(11): 6607-6614.
11. Ramzan, M., Gul, H., Chung, J. D., Kadry, S., & Chu, Y. M. Significance of Hall effect and Ion slip in a three-dimensional bioconvective Tangent hyperbolic nanofluid flow subject to Arrhenius activation energy. *Scientific Reports*, 2020; *10*(1): 18342.
12. Murina F, Vicariotto F, Di Francesco S. Thymol, eugenol and lactobacilli in a medical device for the treatment of bacterial vaginosis and vulvovaginal candidiasis. New

Microbiol, Jul. 2018; 41(3): 220-224. Epub 2018 Jun 6. PMID: 29874389.

13. Mignet N, Seguin J, Chabot GG. Bioavailability of polyphenol liposomes: a challenge ahead. Pharmaceutics, Sep. 17, 2013; 5(3): 457-71. doi: 10.3390/pharmaceutics5030457. PMID: 24300518; PMCID: PMC3836625.
14. Carmo, P. H. F. D., Garcia, M. T., Figueiredo-Godoi, L. M. A., Lage, A. C. P., Silva, N. S. D., & Junqueira, J. C. Metal nanoparticles to combat Candida albicans infections: an update. *Microorganisms*, 2023; *11*(1): 138.
15. Guo, Y. X., & He, Y. X. Nanoparticle-based drug delivery systems: An updated strategy for treating fungal keratitis. *Colloids and Interface Science Communications*, 2024; *61:* 100794. https://doi.org/10.1016/j.colcom.2024.100794
16. Jia, D., & Sun, W. Silver nanoparticles offer a synergistic effect with fluconazole against fluconazole-resistant Candida albicans by abrogating drug efflux pumps and increasing endogenous ROS. *Infection, Genetics and Evolution*, 2021; *93:* 104937.
17. Lara, H. H., Romero-Urbina, D. G., Pierce, C., Lopez-Ribot, J. L., Arellano-Jiménez, M. J., & Jose-Yacaman, M. Effect of silver nanoparticles on Candida albicans biofilms: an ultrastructural study. *Journal of nanobiotechnology*, 2015; *13*(1): 91.
18. Pandian, C. J., Palanivel, R., & Dhanasekaran, S. Screening Antimicrobial Activity of Nickel Nanoparticles Synthesized Using Ocimum sanctum Leaf Extract. *Journal of Nanoparticles*, 2016; *2016:* 1–13. https://doi.org/10.1155/2016/4694367
19. Chouhan, D., Dutta, A., Kumar, A. *et al.* Application of nickel chitosan nanoconjugate as an antifungal agent for combating *Fusarium* rot of wheat. *Sci Rep.*, 2022; 12: 14518. https://doi.org/10.1038/s41598-022-18670-2
20. Madkhali, O. A. A comprehensive review on potential applications of metallic nanoparticles as antifungal therapies to combat human fungal diseases. *Saudi Pharmaceutical Journal*, 2023; *31*(9): 101733. https://doi.org/10.1016/j.jsps.2023.101733
21. Bhoye, M., Pansambal, S., Basnet, P., Lin, K. A., Gutierrez-Mercado, K. Y., Pérez-Larios, A., Chauhan, A., Oza, R., & Ghotekar, S. Eco-Friendly Synthesis of Ni/NiO Nanoparticles Using Gymnema sylvestre Leaves Extract for Antifungal Activity. *Journal of Composites Science*, 2023c*; 7*(3): 105. https://doi.org/10.3390/jcs7030105
22. Roy Choudhury S, Ghosh M, Goswami A. Inhibitory effects of sulfur nanoparticles on membrane lipids of Aspergillus niger: a novel route of fungistasis. Curr Microbiol, Jul. 2012; 65(1): 91-7. doi: 10.1007/s00284-012-0130-7. Epub 2012 Apr 27. PMID: 22538469.
23. Sri Varalakshmi G, Pawar C, Selvam R, Gem Pearl W, Manikantan V, Sumohan Pillai A,

Alexander A, Rajendra Prasad N, Enoch IVMV, Dhanaraj P. Nickel sulfide and dysprosium-doped nickel sulfide nanoparticles: Dysprosium-induced variation in properties, in vitro chemo-photothermal behavior, and antibacterial activity. Int J Pharm., Aug. 25, 2023; 643: 123282. doi: 10.1016/j.ijpharm.2023.123282. Epub 2023 Jul 29. PMID: 37524253.

24. Genchi G, Carocci A, Lauria G, Sinicropi MS, Catalano A. Nickel: Human Health and Environmental Toxicology. Int J Environ Res Public Health, Jan. 21, 2020; 17(3): 679. doi: 10.3390/ijerph17030679. PMID: 31973020; PMCID: PMC7037090.
25. Nachimuthu, S., Sundar, M., Manikavasagam, K., Sadhasivam, B., Veerychetty, V., Ponnusamy, R., & Peraman, M. In vivo Wound Healing Study of Chitosan turmeric films in rat model. *Journal of Chemical and Pharmaceutical Sciences*, 2018; *11*(04): 268–273. https://doi.org/10.30558/jchps.20181104004
26. Farcas, A.D., Mot, A.C., Zagrean-Tuza, C. *et al.* Remarkable rutin-rich *Hypericum capitatum* extract exhibits anti-inflammatory effects on turpentine oil-induced inflammation in rats. *BMC Complement Altern Med.*, 2019; 19: 289. https://doi.org/10.1186/s12906-019-2680-8
27. Moss, G. P., Smith, P. A. S. and Tavernier, D.. "Glossary of class names of organic compounds and reactivity intermediates based on structure (IUPAC Recommendations 1995)" *Pure and Applied Chemistry*, 1995; 67(8-9): 1307-1375. https://doi.org/10.1351/pac199567081307
28. Mezger, T. G. (2012). The Rheology Handbook (4th ed.). Vincentz Network. ISBN 3748600364, 9783748600367
29. Sneen, R. A., & Matheny, N. P. Mechanisms of substitution at unactivated carbon atoms. *Journal of the American Chemical Society*, 1964; *86*(24): 5503–5511. https://doi.org/10.1021/ja01078a023
30. El-Gazzar, N., Elez, R. M. A., Attia, A. S., Abdel-Warith, A. W. A., Darwish, M. M., Younis, E. M., ... & Elsohaby, I. Antifungal and antibiofilm effects of probiotic Lactobacillus salivarius, zinc nanoparticles, and zinc nanocomposites against Candida albicans from Nile tilapia (Oreochromis niloticus), water and humans. *Frontiers in cellular and infection microbiology*, 2024; *14:* 1358270.
31. Kamli, M. R., Alzahrani, E. A., Albukhari, S. M., Ahmad, A., Sabir, J. S., & Malik, M. A. Combination effect of novel bimetallic Ag-Ni nanoparticles with fluconazole against Candida albicans. *Journal of Fungi*, 2022; *8*(7): 733.
32. Pathania, V., Gupta, A. P., & Singh, B. Improved HPTLC Method for Determination of

Curcuminoids from Curcuma longa. *Journal of Liquid Chromatography & Related Technologies*, 2006; *29*(6): 877–887. https://doi.org/10.1080/10826070500531417

33. Lee, K., Choi, S., & Ma, J. Phytochemical Analysis of Curcumin from Turmeric by RP-HPLC. *Asian Journal of Chemistry*, 2013; *25*(2): 995–998. https://doi.org/10.14233/ajchem.2013.13326
34. Ma, S., Moser, D., Han, F., Leonhard, M., Schneider-Stickler, B., & Tan, Y. Preparation and antibiofilm studies of curcumin loaded chitosan nanoparticles against polymicrobial biofilms of Candida albicans and Staphylococcus aureus. *Carbohydrate polymers*, 2020; *241:* 116254.
35. Hajifathali, S., Lesan, S., Lotfali, E., Salimi-Sabour, E., & Khatibi, M. Investigation of the antifungal effects of curcumin against nystatin-resistant Candida albicans. *Dental Research Journal*, 2023; *20*(1): 50.
36. Pawar, H. A., Gavasane, A. J., & Choudhary, P. D. A Novel and Simple Approach for Extraction and Isolation of Curcuminoids from Turmeric Rhizomes. *Advances in Recycling & Waste Management*, 2018; *06*(01). https://doi.org/10.4172/2475-7675.1000300
37. V, V., Jyotsna, N. L., Bakshi, V., Ismail, S., Mohanty, D., T, K., & M, M. Optimization of Extraction of Curcuminoids from Turmeric Powder (Curcuma longa). *Research Journal of Pharmacy and Technology*, 2021; 4615–4620. https://doi.org/10.52711/0974-360x.2021.00802
38. Gizaw, A., Marami, L. M., Teshome, I., Sarba, E. J., Admasu, P., Babele, D. A., ... & Abdisa, K. Phytochemical screening and in vitro antifungal activity of selected medicinal plants against Candida albicans and Aspergillus niger in West Shewa Zone, Ethiopia. *Advances in Pharmacological and Pharmaceutical Sciences*, 2022; *2022*(1): 3299146.
39. Pfaller, M. A., Diekema, D. J., & Sheehan, D. J. Interpretive breakpoints for fluconazole and Candida revisited: a blueprint for the future of antifungal susceptibility testing. *Clinical microbiology reviews*, 2006; *19*(2): 435-447.
40. Slavin, Y. N., & Bach, H. Mechanisms of antifungal properties of metal nanoparticles. *Nanomaterials*, 2022; *12*(24): 4470.
41. Guo, H., Liu, H., Wu, H., Cui, H., Fang, J., Zuo, Z., ... & Zhao, L. Nickel carcinogenesis mechanism: DNA damage. *International journal of molecular sciences*, 2019; *20*(19): 4690.
42. Manasa, P. S. L., Kamble, A. D., & Chilakamarthi, U. Various extraction techniques of Curcumin─A Comprehensive Review. *ACS Omega*, 2023; *8*(38): 34868–34878.

https://doi.org/10.1021/acsomega.3c04205

43. Cameron, K. S., Buchner, V., & Tchounwou, P. B. Exploring the molecular mechanisms of nickel-induced genotoxicity and carcinogenicity: a literature review. *Reviews on Environmental Health*, 2011; *26*(2): 81–92. https://doi.org/10.1515/reveh.2011.012
44. Ahamed, M., & Alhadlaq, H. A. Nickel nanoparticle-induced dose-dependent cyto-genotoxicity in human MCF-7 cells. *OncoTargets and Therapy*, 2014; *7:* 269–280. https://doi.org/10.2147/OTT.S58044
45. Mehanna, S., Hassan, N.H., Ibrahim, M.A. et al. Neurobehavioral and Neuropathological Alterations Induced by Nickel Sulphate Toxicity in Rats: Molecular Mechanisms and Prophylaxis with Curcumin Supplementation. Biol Trace Elem Res., 2025; 203: 6481–6490. https://doi.org/10.1007/s12011-025-04654-6
46. Sahoo, B. K., Ghosh, K. S., Bera, R., & Dasgupta, S. Studies on the interaction of diacetylcurcumin with calf thymus-DNA. *Chemical Physics*, 2008; *351*(1–3): 163–169. https://doi.org/10.1016/j.chemphys.2008.05.008
47. Nafisi, S., Adelzadeh, M., Norouzi, Z., & Sarbolouki, M. N. Curcumin binding to DNA and RNA. *DNA and cell biology*, 2009; *28*(4): 201-208.
48. Liang, R., Senturker, S., Shi, X., Bal, W., Dizdarogluand, M., & Kasprzak, K. S. Effects of Ni(II) and Cu(II) on DNA interaction with the N-terminal sequence of human protamine P2: enhancement of binding and mediation of oxidative DNA strand scission and base damage. Carcinogenesis, 1999; 20(5): 893–898. https://doi.org/10.1093/carcin/20.5.893
49. Zarenezhad E, Abdulabbas HT, Marzi M, Ghazy E, Ekrahi M, Pezeshki B, Ghasemian A, Moawad AA. Nickel Nanoparticles: Applications and Antimicrobial Role against Methicillin-Resistant *Staphylococcus aureus* Infections. Antibiotics (Basel), Sep. 7, 2022; 11(9): 1208. doi: 10.3390/antibiotics11091208. PMID: 36139986; PMCID: PMC9495148.
50. Liu, Y., & Filler, S. G. Candida albicans Als3, a Multifunctional Adhesin and Invasin. *Eukaryotic Cell*, 2010; *10*(2): 168–173. https://doi.org/10.1128/ec.00279-10
51. Mayer, F. L., Wilson, D., Jacobsen, I. D., Miramón, P., Slesiona, S., Bohovych, I. M., Brown, A. J. P., & Hube, B. Small but Crucial: The Novel Small Heat Shock Protein Hsp21 Mediates Stress Adaptation and Virulence in Candida albicans. *PLoS ONE*, 2012; *7*(6): e38584. https://doi.org/10.1371/journal.pone.0038584
52. Lee YS, Chen X, Widiyanto TW, Orihara K, Shibata H and Kajiwara S. Curcumin affects function of Hsp90 and drug efflux pump of Candida albicans. Front. Cell. Infect.

Microbiol, 2022; 12: 944611. doi: 10.3389/fcimb.2022.944611

53. McCrory C, Verma J, Tucey TM, Turner R, Weerasinghe H, Beilharz TH, Traven A. The short-chain fatty acid crotonate reduces invasive growth and immune escape of Candida albicans by regulating hyphal gene expression. mBio., 2023; 14: e02605-23.https://doi.org/10.1128/mbio.02605-23
54. Phan QT, Myers CL, Fu Y, Sheppard DC, Yeaman MR, Welch WH, et al. Als3 Is a Candida albicans Invasin That Binds to Cadherins and Induces Endocytosis by Host Cells. PLoS Biol., 2007; 5(3): e64. https://doi.org/10.1371/journal.pbio.0050064
55. Pandey M, Wasnik K, Gupta S, Singh M, Patra S, Gupta P, Pareek D, Maity S, Tilak R, Paik P. Targeted specific inhibition of bacterial and Candida species by mesoporous Ag/Sn-SnO2 composite nanoparticles: in silico and in vitro investigation. RSC Adv.,m Jan. 5, 2022; 12(2): 1105-1120. doi: 10.1039/d1ra07594b. PMID: 35425144; PMCID: PMC8978812.
56. Shahabadi N, Mahdavi M. Green synthesized silver nanoparticles obtained from Stachys schtschegleevii extract: ct-DNA interaction and in silico and in vitro investigation of antimicrobial activity. J Biomol Struct Dyn, Apr. 2023; 41(6): 2175-2188. doi: 10.1080/07391102.2022.2028680. Epub 2022 Jan 20. PMID: 35048781.
57. Mayer FL, Wilson D, Hube B. Hsp21 potentiates antifungal drug tolerance in Candida albicans. PLoS One. 2013; 8(3): e60417. doi: 10.1371/journal.pone.0060417. Epub 2013 Mar 22. PMID: 23533680; PMCID: PMC3606193.